

# Nonlinear Transformations Against Unlearnable Datasets

Thushari Hapuarachchi<sup>a</sup>, Jing Lin<sup>a</sup>, Kaiqi Xiong<sup>a,\*</sup>, Mohamed Rahouti<sup>b</sup>, Gitte Ost<sup>a</sup>

<sup>a</sup>Department of Mathematics and Statistics, University of South Florida, Tampa, 33613, Florida, USA

<sup>b</sup>Department of Computer and Information Science, Fordham University, New York, Bronx, USA

---

## Abstract

Automated scraping stands out as a common method for collecting data in deep learning models without the authorization of data owners. Recent studies have begun to tackle the privacy concerns associated with this data collection method. Notable approaches include Deepconfuse, error-minimizing, error-maximizing (also known as adversarial poisoning), Neural Tangent Generalization Attack, synthetic, autoregressive, One-Pixel Shortcut, Self-Ensemble Protection, Entangled Features, Robust Error-Minimizing, Hypocritical, and TensorClog. The data generated by those approaches, called “unlearnable” examples, are prevented “learning” by deep learning models. In this research, we investigate and devise an effective nonlinear transformation framework and conduct extensive experiments to demonstrate that a deep neural network can effectively learn from the data/examples traditionally considered unlearnable produced by the above twelve approaches. The resulting approach improves the ability to break unlearnable data compared to the linear separable technique recently proposed by researchers. Specifically, our extensive experiments show that the improvement ranges from 0.34% to 249.59% for the unlearnable CIFAR10 datasets generated by those twelve data protection approaches, except for One-Pixel Shortcut. Moreover, the proposed framework achieves over 100% improvement of test accuracy for Autoregressive and REM approaches compared to the linear separable technique. Our findings suggest that these approaches are inadequate in preventing unauthorized uses of data in machine learning models. There is an urgent need to develop more robust protection mechanisms that effectively thwart an attacker from accessing data without proper authorization from the owners.

*Keywords:* Deep Neural Network, machine learning, generalization attack, unlearnable examples, data augmentation

---

## 1. Introduction

Deep learning typically requires a large dataset to achieve reliable performance, prompting researchers to make significant efforts in scraping data from the Internet. However, the owners of datasets may have a serious concern about the unauthorized use of the databases, including copyright infringement and privacy violations, especially in domains like media streaming and privacy-preserving applications (Shokri et al., 2017). The infringement and violations have inspired a variety of research studies to avoid such a violation of data collection. Among

these, a generalization attack stands out as a prominent method for impeding a deep neural network (DNN) model from effectively learning from a provided dataset. It is a type of data poisoning attack wherein a specific portion of training data (e.g., a portion of data the owners aims to safeguard from unauthorized use) is altered, hindering the learning process and leading to a deficiency of generalization manifested as poor model accuracy on unseen data. It must be pointed out that the significance of data perturbation must be *minor* so that legitimate users can still use the dataset. The crafted data are called *unlearnable datasets* or *unlearnable examples*.

In this research, we investigate twelve well-known approaches to preventing datasets from unauthorized uses by deep learning models. They

---

\*Corresponding author

*Email addresses:* saumya2@usf.edu (Thushari Hapuarachchi), jinglin314@gmail.com (Jing Lin), xiongk@usf.edu (Kaiqi Xiong), mrahouti@fordham.edu (Mohamed Rahouti), gitteost@usf.edu (Gitte Ost)

are Deepconfuse (Feng et al., 2019), error-minimizing (Huang et al., 2021), error-maximizing (also known as adversarial poisoning) (Fowl et al., 2021), Neural Tangent Generalization Attack (NTGA) (Yuan and Wu, 2021), synthetic (Yu et al., 2021), autoregressive (Segura et al., 2022), One-Pixel Shortcut (OPS) (Wu et al., 2023), Self-Ensemble Protection (SEP) (Chen et al., 2022), Entangled Features (EntF) (Wen et al., 2023), Robust Error-Minimizing (REM) (Fu et al., 2022), Hypocritical (Tao et al., 2021), and TensorClog (Shen et al., 2019) approaches. These approaches can be formulated as a bi-level optimization, which is usually very difficult to be solved efficiently unless the learning model is convex (Koh and Liang, 2017; Jagielski et al., 2018). For instance, the error-minimizing approach makes personal data completely unusable by solving a min-min optimization problem, in which an iterative process is developed to minimize the training loss with respect to the  $L_p$ -norm bounded noise and model weights, respectively.

As pointed out by Yu et al. (2021), unlearnable perturbations can effectively disrupt DNN training due to linear separability. However, not all existing unlearnable perturbations exhibit this characteristic as revealed in Segura et al. (2023). Additionally, the authors present an attack on unlearnable data leveraging the linear separability inherent in such perturbations, referred to as the *orthogonal projection attack* (OPA). Nevertheless, their findings suggest that the effectiveness of OPA diminishes when applied to nonlinear perturbations like autoregressive ones in Segura et al. (2022).

In this paper, we explore twelve advanced data protection approaches. Our main contributions include:

- Propose an effective nonlinear transformation framework designed to circumvent data protection measures, thereby facilitating the training of DNNs on augmented, previously deemed unlearnable data. The proposed framework applies to any machine learning model and data.
- The proposed nonlinear transformation framework improves the linear separable technique given in Segura et al. (2023) for all twelve data protection approaches, except for OPS in Wu et al. (2023). The improvement is very significant for the six approaches: NTGA, Deepconfuse, Error-minimizing, Error-maximizing, Autoregressive, and REM. In particular, the pro-

posed framework achieves over 100% improvement in test accuracy for Autoregressive and REM compared to the linear separable technique.

- Demonstrate through extensive experiments that the nonlinear transformation technique diminishes the efficacy of data protection strategies, empowering DNNs to acquire knowledge from previously deemed 'unlearnable' data with an accuracy comparable to training on pristine data. This underscores the shortcomings of existing data protection methods.
- Illustrate experimentally that data protection methods can be circumvented by incorporating clean data from external sources (or partially perturbed data). This underscores the necessity for future data protection strategies to address and mitigate these vulnerabilities.

## 2. Preliminaries

Various data poisoning attacks can target machine learning algorithms, with our specific emphasis here on generalization attacks. In the context of a generalization attack, adversaries endeavor to manipulate the dataset, disrupting the training process of the DNN model. The ultimate goal is to yield a model with compromised generalizability or diminished capacity for generalization.

Generalization attacks on machine learning models is contingent upon the adversary's ability to manipulate the training data. They are broadly classified into two categories: dirty-label attacks and clean-label attacks. This study primarily focuses on clean-label-based generalization attacks, as a substantial portion of web data is typically unlabeled before the data collection process.

**Definition 2.1** (Clean-label generalization attack). Let  $D = (X_D, Y_D)$  be a training set, where  $X_D \in \mathbb{R}^{n \times d}$  is a set of training images,  $n \in \mathbb{N}$  is the number of training images, and  $d \in \mathbb{N}$  is the dimension of training images;  $Y_D \in \mathbb{R}^{n \times c}$  is a set of training outputs and  $c \in \mathbb{N}$  is the dimension of training labels. Similarly, we denote a validation set by  $V = (X_V, Y_V)$ , where  $m \in \mathbb{N}$  is the number of validation images,  $X_V \in \mathbb{R}^{m \times d}$  is a set of validation images, and  $Y_V \in \mathbb{R}^{m \times c}$  is a set of validation labels. Let  $f(\cdot; \theta)$  be a machine learning model parameterized by  $\theta$ . Then, the generalization attack generates the "unlearnable examples" by solving the following bi-level optimization problem (Yuan and Wu,

2021):

$$\arg \max_{\|g_\xi(X_D)\|_p \leq \epsilon} \mathcal{L}_V(f(X_V; \theta^*), Y_V) \quad (1)$$

subject to  $\theta^* \in \arg \min_{\theta} \mathcal{L}_D(f(X_D + g_\xi(X_D); \theta), Y_D)$ ,

where  $\mathcal{L}_V$  and  $\mathcal{L}_D$  are the loss functions of validation and training sets, respectively;  $g_\xi$  is a noise generator characterized by the weight parameter  $\xi$ , and  $\epsilon$  represents the maximum allowable perturbation or noise specified by a user. Since  $g_\xi$  is only added to  $X_D$  in (1) and the label  $Y_D$  is not modified, it is called a *clean-label generalization attack*.

A trivial solution to the bi-level optimization problem (1) is to alternatively update  $\theta^*$  over poisoned data  $X_D + g_\xi(X_D)$  by using the gradient *descent* method and update  $g_\xi$  over clean validation data  $X_V$  by using the gradient *ascent* method. However, achieving convergence of both weight parameters  $\theta^*$  and  $g_\xi$  is intractable in practice. Over the past few years, various data protection approaches have been introduced to solve this bi-level optimization problem.

### 2.1. Data Protection Approaches

We introduce several well-known data protection approaches.

**Deepconfuse:** Feng et al. (2019) proposed the Deepconfuse approach to solving a simpler version of the bi-level optimization problem (1). They relaxed the constraint in (1) by decoupling the alternating update procedure for stability and memory efficiency to avoid the storage of the gradient update of  $\theta_i$  and model  $g_\xi$  as an auto-encoder. Their objective is to find a noise generator  $g_{\xi^*}$  that results in a classifier,  $f$ , with the worst test accuracy.

**Error-minimizing:** This approach in Huang et al. (2021) makes data unlearnable for a deep learning model by minimizing the training loss. The model can no longer learn anything from these examples since the training loss is close to zero. Hence, this approach protects against the unauthorized exploitation of the data. The following min-min bi-level optimization problem generates error-minimizing noise  $\delta$  to inject into clean training input  $D$  in order to make  $D$  unusable for DNNs (Huang et al., 2021):

$$\min_{\theta} \left[ \min_{\delta} \mathcal{L}_D(f(X_D + \delta; \theta), Y_D) \right], \quad (2)$$

subject to

$$\|\delta\|_p \leq \epsilon,$$

where  $\delta = [\delta_1, \delta_2, \dots, \delta_n]$  is the perturbation. Both the noise  $\delta$  and the weight parameter  $\theta$  are found by minimizing the classification loss  $\mathcal{L}_D$ .  $x'_i = x_i + \delta_i$  is the  $i$ -th unlearnable example. According to Huang et al. (2021), this type of noise is called *sample-wise noise* since the noise is generated separately for each example. They also proposed *class-wise noise*, where all examples in the same class have the same noise.

To solve this min-min bi-level optimization problem (2), they proposed an iterative algorithm by repeatedly performing  $M$  steps of optimization for  $\theta$  (this is the regular model training), followed by calculating  $\delta$  over  $D$  based on the Projected Gradient Descent (PGD) in Madry et al. (2018). The iterative process stops once the error rate falls below the threshold defined by the user-specified parameter  $\lambda$ .

Fowl et al. (2021) decided not to solve the general bi-level problem (1) but instead solved the following empirical loss maximizing problem:

$$\max_{\|\delta\|_p \leq \epsilon} \left[ \mathcal{L}_D(f(X_D + \delta; \theta^*), Y_D) \right], \quad (3)$$

where  $\theta^*$  denotes the parameters of a model trained on clean data (Fowl et al., 2021). Most attacks in Fowl et al. (2021) are bounded by  $l_\infty$ -norm with  $\epsilon = 8/255$ . The optimization problem (3) is solved with 250 steps of PGD. Fowl et al. (2021) also used differentiable data augmentation when crafting the poisons.

Fowl et al. (2021) further introduced a variant of (3), called the class targeted adversarial attack:

$$\max_{\|\delta\|_p \leq \epsilon} \left[ \mathcal{L}_2(f(x_i + \delta_i; \theta^*), g(y_i)) \right], \quad (4)$$

where  $g$  is a permutation on the label space. For crafting class targeted attacks, they labeled  $i \rightarrow i + 3$  for CIFAR-10 (Fowl et al., 2021).

**NTGA:** Before describing NTGA, we first review the Neural Tangent Kernel (NTK), which was introduced by Jacot et al. (2018). NTK is a kernel describing the DNN evolution during the training by gradient descent. NTK becomes a constant in the infinite-width limit for most common neural network models (i.e., architectures) and enables the examination of neural network models through kernel methods-based theoretical tools.

Using the Gaussian process  $\tilde{f}$  with a deterministic kernel to approximate a class of wide neural networks, Yuan and Wu (2021) simplified the bi-

level optimization problem in (1) as:

$$\arg \max_{\|g_\xi(X_D)\|_p \leq \epsilon} \mathcal{L}_V(\bar{f}(X_V, X_D, g_\xi(X_D), Y_D, t), Y_V), \quad (5)$$

where  $t$  is the time step at which an attack takes effect during training. This eliminates the need to find the weight parameter  $\theta$  or know the model architecture. This optimization problem can be easily solved with the projected gradient ascent without iterating through the training steps, as in Deepconfuse attacks (Feng et al., 2019).

**Synthetic:** Observing that the advanced techniques described above generate almost linear separable perturbations, Yu et al. (2021) developed a two-stage process to protect the data. First, they randomly generated some normally distributed noise  $\eta$ , for some integer  $k$  such that  $s^2 = k * p^2$ , where  $s \times s$  is the image dimension and  $p \times p$  is patch dimension (Yu et al., 2021). Then, they cut that image into  $k$  patches, where each element in patch  $i$  has the same value, which is the  $i$ -th element of  $\eta$ . These patches together consist of synthetic noise for that image.

**Autoregressive:** Segura et al. (2022) crafted perturbations using autoregressive (AR) processes, resulting in unlearnable data resistance to common defenses such as adversarial training and “strong” data augmentations; e.g., CutMix, Cutout, and Mixup (Yun et al., 2019). Unlike error-minimizing and error-maximizing noise, AR perturbations do not involve a surrogate model; hence, they are faster to generate. AR perturbations are crafted by using the linear dependence on neighboring pixels. Equation (6) represents an AR process based on  $p$  past observations, denoted by  $AR(p)$ . It forms a filter with a size of  $(p + 1)$  using elements  $\beta_p, \dots, \beta_1$ , and assigns a value of  $-1$  to the  $(p + 1)^{th}$  entry of the filter. Segura et al. (2022) refer to this filter as an AR filter:

$$x_t = \beta_1 x_{t-1} + \beta_2 x_{t-2} + \dots + \beta_{p-1} x_{t-p+1} + \beta_p x_{t-p} + \epsilon_t \quad (6)$$

**Other approaches:** In addition to these approaches, there are other ways to generate unlearnable data. Notably, Fu et al. (2022) proposed an extended version of training examples’ error reduction called *robust error-minimizing noise*. In contrast to error-minimizing noise, robust error-minimizing noise provides defense against adversarial training. Moreover, Wang et al. (2021) crafted a noise called ADversarially Inducing Noise (ADVIN) to make data unlearnable using robust features resistant

to adversarial training. After showing that error-maximizing noise is ineffective against unsupervised contrastive learning models, He et al. (2022) introduced a novel data protection approach against contrastive learning models. Further, Sadasivan et al. (2023b) proposed a filter-based poisoning attack using convolutional filters that can craft successful unlearnable datasets. Recently, Wu et al. (2022) studied unlearnable examples and proposed the One-Pixel Shortcut attack, a model-free technique to generate unlearnable samples. They modified a single pixel from every image, which fools DNN models during training. CUDA in Sadasivan et al. (2023a) is another recently proposed method to protect data from unauthorized use. It adds protection by blurring images using randomly generated class-wise convolutional filters.

## 2.2. Orthogonal Projection Attack (OPA)

Segura et al. (2023) proposed an attack against the data protection approaches discussed in section 2.1. They challenged the notion that unlearnable perturbations must exhibit linear separability across classes for effective exploitation in Yu et al. (2021). They demonstrated it using a counter example, autoregressive perturbations, which defy linear separability. However, OPA relies on linear separability to break unlearnable perturbations.

Initially, Segura et al. (2023) trained a linear logistic regression model on the unlearnable dataset to capture linear features in the data. Then, they performed QR decomposition on the obtained feature matrix. The resulting Q matrix can be considered the orthonormal basis of the captured linear space. Subsequently, unlearnable images are orthogonally projected into this space, effectively removing the linear features from the images. This results in the recovery of the unlearnable images.

Additionally, they demonstrated that their approach is more effective against class-wise linearly separable perturbations, such as OPS in Wu et al. (2022), and synthetic examples in Yu et al. (2021) but less effective against nonlinear perturbations, such as autoregressive. Hence, our study intends to employ nonlinear transformations to break such complex unlearnable perturbations.

## 3. Methodology

Data manipulation has become a pervasive technique across diverse research problems, yet leveraging it effectively to address various challenges remains a formidable and intricate task. This research meticulously examines the characteristics of each nonlinear transformation, identifying specific

methods employed to address challenges of breaking unlearnable datasets.

### 3.1. The Proposed Framework

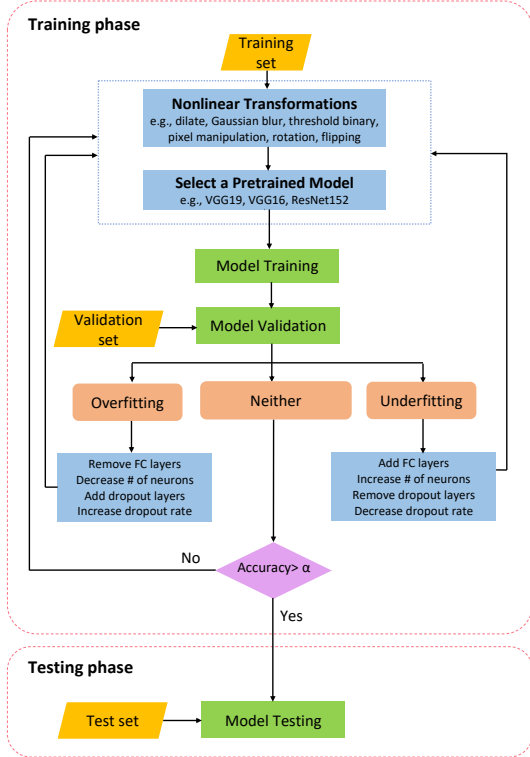


Figure 1: The proposed framework consisting of Nonlinear Transformations, Model Selection, Model Training, Model Validation, and Model Testing.  $\alpha$  is the expected or predefined accuracy.

To examine and identify each nonlinear transformation, we propose a framework that consists of Nonlinear Transformations, Model Selection, Model Training, Model Validation, and Model Testing, depicted in Fig. 1. Initially, we apply nonlinear transformations to a given unlearnable training dataset. Our primary utilization of nonlinear transformations relies on the Open Source Computer Vision Library (OpenCV), a python package for computer vision. Those nonlinear transformations include dilate (Gonzalez and Woods, 2008), Gaussian blur (Chen and Ma, 2009), erode (Haralick et al., 1987), threshold binary (Komarudin et al., 2015), threshold binary inverse (Gervasi et al., 2013), and pixel manipulation (Chaumette et al., 2012). Additionally, for rotation, horizontal flipping, and

other transformations, we employ the Keras ImageDataGenerator (Rahmatullah et al., 2021). These transformations effectively augment the dataset size for training purposes. Subsequently, a pretrained model such as VGG19, VGG16, or ResNet152 is selected. While using a pretrained model is not mandatory, it is commonly convenient. In our experiments, a pretrained model is employed in all cases except for the unlearnable MNIST experiment.

After selecting a pretrained model, we enhance it by incorporating additional fully connected (FC) layers and dropout layers (Srivastava et al., 2014), as required. Subsequently, the modified model undergoes training using the expanded dataset from the initial augmentation step. Following training, we assess the model using the provided validation dataset. In cases where the model exhibits signs of underfitting or overfitting, corrective measures can be taken based on the available options outlined in Fig. 1. With a validation accuracy surpassing a threshold value  $\alpha$ , we proceed to evaluate its performance on the test set. If the validation accuracy falls below expectations, we may explore alternative nonlinear transformations on the training set or consider increasing model complexity (e.g., transitioning from VGG16 to VGG19) to bolster learning capabilities. In the presence of underfitting or overfitting issues, adjustments to the model architecture, learning rate, batch size, and number of epochs can be made as necessary. Additionally, exploring different pretrained models is an alternative option.

### 3.2. Breaking Unlearnable Datasets

The pivotal stage in the proposed framework involves identifying suitable nonlinear transformations to address unlearnable datasets, a task characterized by its challenges and time-intensive nature. This endeavor can be conceptualized as solving the following optimization problem:

$$\arg \min_A \max_{\|g_\xi(X_D)\|_p \leq \epsilon} \mathcal{L}_V(f(X_V; \theta^*), Y_V) \quad (7)$$

subject to  $\theta^* \in \arg \min_{\theta} \mathcal{L}_D(f(A(X_D + g_\xi(X_D)); \theta), Y_D)$ ,

where  $\mathcal{A}$  represents a set of nonlinear transformations and  $A$  is a vector of those transformations whose  $i$ -th element is  $a_i \in \mathcal{A}$  and represents the data augmentation technique applies to  $i$ -th image in  $X_D + g_\xi(X_D)$ . The goal of nonlinear transformations is to expand a training set by using

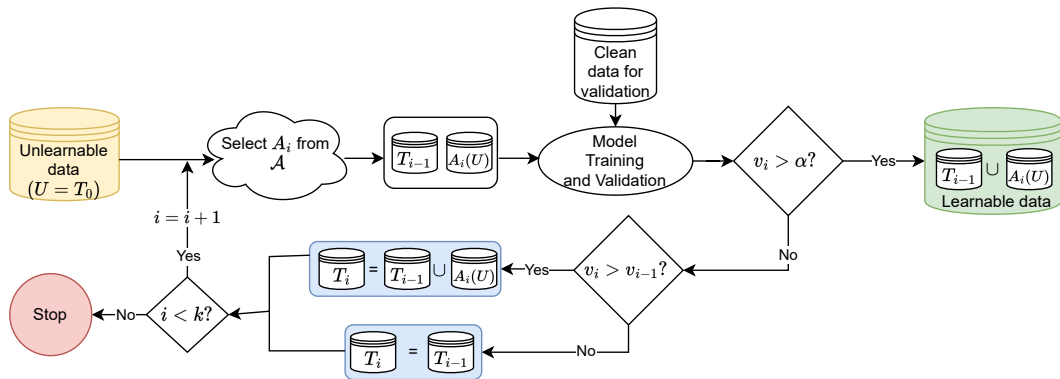


Figure 2: Graphical illustration of the proposed procedure for breaking an unlearnable dataset. In each iteration  $i$  ranging from 1 to  $k$ , a nonlinear transformation,  $A_i$ , is applied to the unlearnable dataset ( $U$ ) from the collection ( $\mathcal{A}$ ), denoted as  $A_i(U)$ . The model is then trained on the augmented dataset, and validation is carried out on a clean validation dataset. If there's an improvement in validation accuracy compared to the previous iteration, the augmented dataset is incorporated into the training set. Here,  $v_i$  represents the validation accuracy in the  $i^{\text{th}}$  iteration, with  $v_0$  being the validation accuracy of the model trained on the initial unlearnable dataset.

---

**Algorithm 1** Generating A Learnable Training Set

---

- 1: **Input:** Unlearnable training set ( $U$ ), Clean validation set, Pretrained model ( $M$ ), Number of iterations ( $k$ ), Space of nonlinear transformations:  $\mathcal{A} = \{A_1, A_2, \dots\}$ , and Target accuracy ( $\alpha$ )
  - 2: **Output:** Augmented learnable training set ( $L$ )
  - 3:  $L \leftarrow U$
  - 4: Train  $M$  on  $L$  and obtain validation accuracy  $v_0$
  - 5: **for**  $i = 1$  **to**  $k$  **do**
  - 6:    $T_i \leftarrow L + A_i(U)$  {The augmented training set  $T_i$ }
  - 7:   Train  $M$  on  $T_i$  and obtain validation accuracy  $v_i$
  - 8:   **if**  $v_i > \alpha$  **then**
  - 9:      $L \leftarrow T_i$
  - 10:    **Break** the loop
  - 11:    **else if**  $v_{i-1} < v_i$  **then**
  - 12:      $L \leftarrow T_i$
  - 13:    **else**
  - 14:      $L \leftarrow L$
  - 15:    **end if**
  - 16: **end for**
- 

class-preserving conversions such as threshold binary (Dao et al., 2019; Qiu et al., 2021).

Solving the optimization problem in (7) is intractable, so we present a heuristic approach (Algorithm 1) to find a set of proper nonlinear transformations. This algorithm provides a procedure for discovering nonlinear transformations to break an unlearnable dataset. Its time complexity is  $k$  times that of the sum of the training and validation times for the model  $M$ . Fig. 2 graphically illustrates this procedure.

Our initial step involves choosing a nonlinear transformation from the spectrum available. Then, we systematically expand the training set by applying each transformation sequentially. It is pivotal to visually inspect a sample of augmented data at each step, as not all techniques yield meaningful images for every dataset. For instance, Threshold Binary and Threshold Binary Inverse transformations may not generate meaningful images for the CIFAR-10 dataset.

Following the application of each technique, we assess the model's performance by obtaining validation accuracy. The validation data remain unperturbed (clean). If there is an improvement in validation accuracy, we retain the expanded dataset for the subsequent iteration. The process continues until the model achieves the target accuracy ( $\alpha$ ), at which point we conclude the dataset expansion.

In implementing the aforementioned method, we predominantly employed conventional nonlinear transformations, encompassing threshold bi-

nary, threshold binary inverse, color channel manipulation, erode, dilate, and Gaussian blur. Threshold binary and threshold binary inverse are commonly applied to grayscale images but can also be used in color images to delineate the primary object from its background. Color channel manipulation is akin to grayscale transformation, involving alterations to the values of one or more color channels in diverse ways.

### 3.3. Nonlinear Transformations

**Threshold binary:** We know that a single number represents the pixel value for a gray image, whereas three numbers on the RGB scale represent the pixel value of a colored image. Although two different types of pixel values are used in gray and colored images, respectively, there is no difference between both types of images when the threshold binary approach is applied. First, we need to define a threshold value and the maximum value of a pixel. When a pixel value is lower than the predefined threshold, the pixel value will be zero. Otherwise, the pixel will be set to the maximum value. For grey images with a pixel value of  $a$ , a threshold value of  $t$ , and a maximum value of  $m$ , let  $npv$  represent a new pixel value. Then, based on the threshold binary approach,  $npv$  is defined as 0 if  $a \leq t$  or  $m$  if  $a > t$  (Harris et al., 2020b).

Similarly, for colored images with a pixel value of  $(r, g, b)$ , a threshold value of  $t$ , and a maximum value of  $m$ ,  $npv = (nr, ng, nb)$  is the new pixel value, where  $nr$ ,  $ng$ , and  $nb$  are the new values of  $r$ ,  $g$ , and  $b$ , respectively. Thus, according to the threshold binary approach, they are defined as:

$$\begin{aligned} nr &= \begin{cases} 0, & \text{if } r \leq t \\ m, & \text{if } r > t, \end{cases} & ng &= \begin{cases} 0, & \text{if } g \leq t \\ m, & \text{if } g > t, \end{cases} \\ nb &= \begin{cases} 0, & \text{if } b \leq t \\ m, & \text{if } b > t \end{cases} \end{aligned} \quad (8)$$

We use threshold binary only for normalized datasets generated by NTGA. The pixel values for those images range from 0 to 1; therefore, we used 1 as our maximum value, corresponding to a value of 255 on non-normalized images<sup>1</sup>. The `cv2.threshold` function with the threshold method argument is set to `cv2.THRESH_BINARY`,

<sup>1</sup><https://www.geeksforgeeks.org/python-thresholding-techniques-using-opencv-set-1-simple-thresholding/>

and it is used for the experiment. See Fig. 3 for an example image based on different data transformations.

**Threshold binary inverse:** In OpenCV, the threshold binary inverse function has the same principle as the threshold binary function (Harris et al., 2020a). The only difference is that the pixel will receive a zero value when it is higher than the threshold value; otherwise, it will receive a maximum value. The `cv2.threshold` function with the threshold method argument is set to `cv2.THRESH_BINARY_INV`, and it is used for the experiment. The first three arguments are the same as for the threshold binary function. Please see Fig. 3 for an example image based on this data argument technique.

**Color channel manipulation:** It is another technique typically used for pixel manipulation in our experiment. An image consists of multiple pixels that contain information about the color of a minute area in that image. Each pixel of a colored image is composed of three values representing the intensity of blue (b), green (g), and red (r) light colors, respectively. However, each pixel of a grey image has only one value representing the light intensity of an image. Color channel manipulation is about changing the color value of one or more color channels. In our experiments, we used color channels to manipulate the pixels based on the code available for operations on images<sup>2</sup>. For instance, when using the `cv2.merge((b,b,b))`, all three channels' values are replaced by the blue channel's value b. In the original image shown in Fig. 4, the sky is blue, indicating that the blue channel value is the largest among all three values for each pixel in the sky area. When `cv2.merge((b,b,b))` replaces three channels with that value b, the blue sky in the original image looks paler in the last image (as shown in Fig. 4) because the purer blue it is, the closer the value is to (255, 255, 255), indicating a white pixel.

Further, sky pixels have low red and green channel values. When those values are used for all three channels shown in the second and third images of Fig. 4, respectively, pixels will get closer to black color since the black is indicated by (0, 0, 0). Color channel manipulations efficiently generate additional images with a negligible computation overhead effort.

<sup>2</sup>[https://docs.opencv.org/4.x/d3/df2/tutorial\\_py\\_basic\\_ops.html](https://docs.opencv.org/4.x/d3/df2/tutorial_py_basic_ops.html)

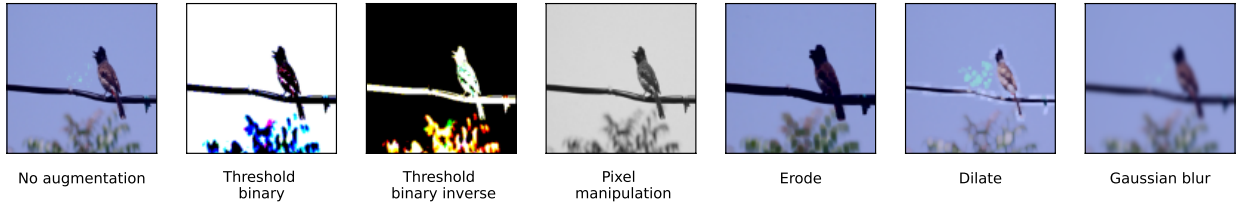


Figure 3: An illustration of nonlinear transformation techniques.

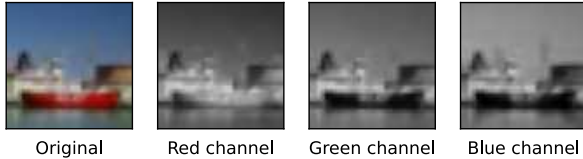


Figure 4: An illustration of the color channels.

**Erode:** This is a commonly used image-processing technique introduced in mathematical morphology. This technique was initially defined for binary images (black and white), but it was later extended to grayscale images. Erosion reduces bright areas of an image and replaces them with dark regions (Haralick et al., 1987). Consider  $A$  and  $B$  as sets in  $\mathbb{Z}^2$ , where  $A$  is considered as the coordinates of an input image, and  $B$  denotes the structuring element or the shape parameter. Haralick et al. (1987) denote the translation of  $B$  by  $x \in \mathbb{Z}^2$  as  $(B)_x$  as follows:

$$(B)_x = \{c \in \mathbb{Z}^2 | c = b + x, \exists b \in B\}. \quad (9)$$

Then, Haralick et al. (1987) defined erosion in the following way.

**Definition 3.1.** The erosion of  $A$  by  $B$  ( $A \ominus B$ ) is defined as:

$$A \ominus B = \{x | (B)_x \subseteq A\}. \quad (10)$$

The erosion of  $A$  by  $B$  is the set of points  $x$  such that the translation of  $B$  by  $x$  is contained in  $A$ . In other words, the erosion of  $A$  by  $B$  includes the points that translate  $B$  in a way such that translated  $B$  does not have any points outside  $A$  (Gonzalez and Woods, 2008). In a programming setting, structuring element  $B$  is known as a kernel. Based on the kernel, we can control the severity of erosion. We used `cv2.erode` in OpenCV for the erode transformation, which has three main arguments. The first argument is a base image ( $A$ ). The second argument is a kernel,  $B$ . We define the kernel as an all-ones matrix that slides across  $A$ . If all pixels

under the kernel are 1, the original pixel value will be converted to 1; otherwise, the pixel value is 0. In that way, the white region of an original image will be reduced. The third argument in this function is the number of iterations. It specifies how many times we want to perform this transformation.

**Dilate:** Dilate is the dual transform of erode. Dilation is also mainly introduced to binary images. As the name reveals, a dilate transformation grows or expands the bright region of an image into a black area in the background of an image (Haralick et al., 1987). Haralick et al. (1987), define dilation transformation as follows.

**Definition 3.2.** The dilation of  $A$  by  $B$  ( $A \oplus B$ ) is defined by:

$$A \oplus B = \{c \in \mathbb{Z}^2 | c = a + b, \exists a \in A \text{ and } \exists b \in B\}. \quad (11)$$

In our experiments, we performed a dilate transformation based on `cv2.dilate` in OpenCV. A dilate function also has the same arguments as an erode function, i.e., a base image, a kernel, and the number of iterations. Like the erode function, the kernel is specified as an all-ones matrix and slides cross  $A$ . However, it does not perform the same way as erode. If at least one of the pixels under the kernel is 1, the original pixel value will be converted to 1; otherwise, the pixel value is 0. This transformation will expand the white region of an image.

**Gaussian blur:** The Gaussian blur transformation of a pixel value is computed by taking the weighted average of neighboring pixel values. A Gaussian blur transformation is carried out by the convolution that involves a kernel generated using a Gaussian function. A Gaussian function is defined as follows:

$$h(x, y) = K \exp \left\{ \frac{-(x^2 + y^2)}{2\sigma^2} \right\}, \quad (12)$$

where  $K$  is a normalization constant,  $x$  and  $y$  are distances from the original pixel to its neighbor

pixel in horizontal and vertical axes, respectively, and  $\sigma$  denotes the standard deviation of  $(x, y)$ , which controls the intensity of the blur. For our experiments, we conducted a Gaussian blur transformation by using `cv2.GaussianBlur` in OpenCV. Similar to dilate and erode, we need to specify the size of a kernel before applying a Gaussian blur transformation. For example, based on extensive experiments, we chose a kernel with length of 55 and width of 5 in this research.

#### 4. Experimental Evaluation

We have empirically demonstrated, through extensive experiments and analysis, that major data protection approaches—namely, Deepconfuse (Feng et al., 2019), error-minimizing noise approach (Huang et al., 2021), error-maximizing noise approach (Fowl et al., 2021), NTGA (Yuan and Wu, 2021), synthetic approach (Yu et al., 2021), autoregressive noise approach (Segura et al., 2022), OPS (Wu et al., 2023), SEP (Chen et al., 2022), EntF (Wen et al., 2023), REM (Fu et al., 2022), Hypocritical (Tao et al., 2021), and TensorClog (Shen et al., 2019)—can be effectively circumvented by leveraging the proposed framework outlined in Section 3. We have extensively investigated the learnability of the twelve data protection approaches using the CIFAR-10 (Krizhevsky et al., 2009) dataset. We selected CIFAR-10 since it is the standard dataset used by many unlearnable example researchers. Additionally, we apply our framework to two other benchmark datasets: MNIST (LeCun and Cortes, 2010) and ImageNet (Deng et al., 2009) generated by NTGA. Those results are presented in Section 5.

##### 4.1. The Proposed Framework on the Twelve Unlearnable Approaches

We aim to reveal that the unlearnable CIFAR-10 datasets created by the twelve popular data protection approaches, i.e., NTGA (Yuan and Wu, 2021), Deepconfuse (Feng et al., 2019), error-minimizing (Huang et al., 2021), error-maximizing (Fowl et al., 2021), synthetic (Yu et al., 2021), autoregressive (Segura et al., 2022), OPS (Wu et al., 2023), SEP (Chen et al., 2022), EntF (Wen et al., 2023), REM (Fu et al., 2022), Hypocritical (Tao et al., 2021), and TensorClog (Shen et al., 2019) are also vulnerable to our proposed approach. In our work, the datasets generated by Deepconfuse, error-minimizing, error-maximizing, and synthetic approaches were obtained from Yu et al. (2021). Yuan and Wu (2021) publicly released three unlearnable datasets:

MNIST, CIFAR-10, and ImageNet on Kaggle. We utilized these data to demonstrate the vulnerability of NTGA perturbations to our approach. The datasets created by other approaches—autoregressive, OPS, SEP, EntF, REM, Hypocritical, and TensorClog—were generated using the available code in their respective GitHub repositories.

For all the datasets, we used Tensorflow’s pre-trained VGG models initialized with ImageNet weights. Table 4 explicitly mentions the nonlinear transformations and model specifications used in each unlearnable dataset based on the proposed framework, where we conducted extensive experiments for all those twelve data protection approaches studied in this paper. Column 2 gives the transformations used to expand the training dataset. In this table, Column 3 includes the attributes used for Keras ImageDataGenerator to conduct more transformations during the training process. Last three columns specify the model specifications.

Table 1 summarizes our study’s main findings, with column 2 displaying test accuracies mostly below 30% for models trained on these data protection approaches. To demonstrate the ability to learn from the so-called unlearnable dataset, we employed our nonlinear transformation approach detailed in Section 3. Its resulting accuracy is given in Column 4. Column 3 shows the test accuracy of the models trained on the same unlearnable datasets using linear transformation technique, specifically OPA in Segura et al. (2023). We employed the code provided in their GitHub repositories with default settings, such as a non-pretrained ResNet18 model under PyTorch platform. Column 5 gives the difference between the test accuracies of our approach and the orthogonality projection attack. The performance difference is shown as a percentage in Column 6. The last column shows the accuracy after PGD adversarial training Fu et al. (2022), which is another widely used method to break unlearnability.

**NTGA (Yuan and Wu, 2021):** We illustrate the effectiveness of our proposed framework in countering the unlearnable CIFAR-10 data generated by NTGA Yuan and Wu (2021). As reported in Yuan and Wu (2021), the lowest test accuracy for the unlearnable CIFAR-10 data is approximately 41%. We aim to demonstrate that the unlearnable CIFAR-10 crafted by NTGA becomes learnable applying our proposed framework. We used the proposed nonlinear transformation based

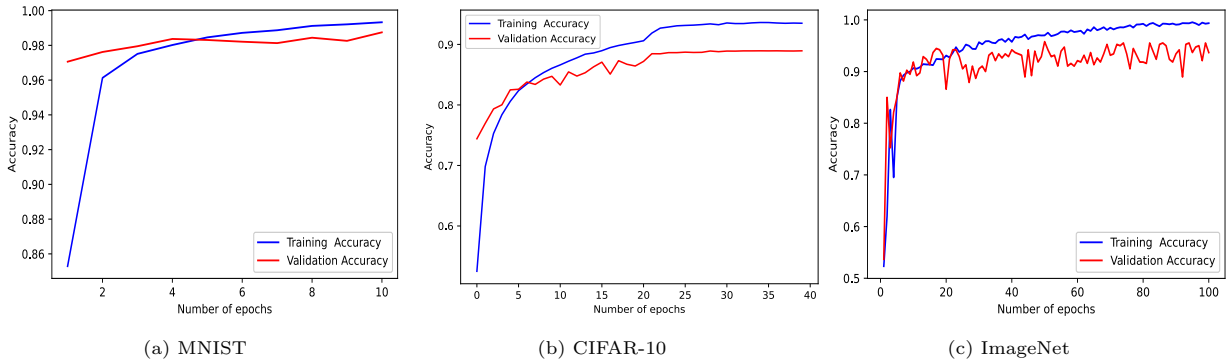


Figure 5: The training and validation accuracy of the model trained with unlearnable data created by NTGA.

Data protection approach	No defense	OPA	Our approach	Performance difference	% Improvement	Adversarial training
NTGA	40%	61.54%	88.74%	27.20%	44.20%	84.75%
Deepconfuse	29%	75.28%	87.0%	11.72%	15.57%	84.92%
Error-minimizing	20%	69.18%	85.2%	16.02%	23.16%	79.68%
Error-maximizing	6%	75.57%	92.2%	16.63%	22.01%	85.36%
Synthetic	13%	87.90%	88.2%	0.30%	0.34%	86.74%
Autoregressive	11%	25.59%	86.9%	61.31%	239.59%	80.54%
OPS	15%	88.10%	86.71%	-1.39%	-1.58%	13.01%
SEP	23%	87.28%	88.18%	0.9%	1.03%	87.20%
EntF	71%	85.67%	88.59%	2.92%	3.41%	82.30%
REM	27%	34.78%	85.70%	50.92%	146.41%	49.51%
Hypocritical	19%	86.79%	89.68%	2.89%	3.33%	80.41%
TensorClog	48%	88.05%	88.84%	0.79%	0.90%	85.16%

Table 1: The baseline test accuracy is given in Column 2 whose results are extracted from those papers that presented their respective approaches given Column 1. Our approach in column 4 performs higher test accuracy than OPA, a linear transformation technique, given in Column 3 for all the twelve approaches except OPS, where six of them are remarkably better. Our experimental results in Column 4 also suggest that these twelve data protection approaches remain vulnerable to nonlinear transformations. While Column 5 gives the performance difference between our nonlinear transformation approach and OPA (a linear transformation approach) in Segura et al. (2023), Column 6 presents the performance improvement percentages of our approach compared to OPA. Our research also adopted the adversarial training method in Fu et al. (2022) for model training, and Column 7 gives resulting test accuracy for the trained models. Columns 6 and 7 clearly demonstrates that our approach can achieve comparable test accuracy like the adversarial training method, while our approach performs much better for OPS.

framework to increase our training dataset size, enhancing the model’s resilience to image transformations. Notably, color channel manipulation tripled the training dataset size. Additionally, we utilized Keras’s built-in ImageDataGenerator on the training dataset for further augmentation, incorporating a zoom range of 0.3, a rotation range of 7, a width shift range of 0.35, a height shift range of 0.35, horizontal flipping, and a shear range of 0.4. For a baseline model, we conducted experiments based on a Visual Geometry Group (VGG) in Simonyan and Zisserman (2015). There are several variants in VGG models depending on the number of convolutional layers. After thorough experiments with

VGG16, VGG19, and ResNet50, we selected the VGG19 model with ImageNet pretrained weights from Keras for its superior baseline performance. We enhanced the model by incorporating four fully connected (FC) layers and two dropout layers, randomly dropping 30% of the weights after each of the first two FC layers. The ReLU activation function (Agarap, 2018) is employed for every FC layer, except for the output layer, which uses softmax activation with ten neurons. Refer to Table 2b for detailed model architecture. The model was trained for 40 epochs with a learning rate of 0.008, resulting in a test accuracy of 88.74%, a validation accuracy of 88.94%, and a training accuracy of 93.50%. Fig.

Layer	Output shape	Activation function
Input	28 x 28 x 1	
Convolutional	28 x 28 x 32	ReLU
Max pool	14 x 14 x 32	
Convolutional	14 x 14 x 64	ReLU
Max pool	7 x 7 x 64	
Flatten		
FC	1024	ReLU
Dropout (0.25)		
FC	10	Softmax

(a) MNIST

Layer	Output shape	Activation function
Input	32 x 32 x 3	
2 x Convolutional	32 x 32 x 64	ReLU
Max pool	16 x 16 x 64	
2 x Convolutional	16 x 16 x 128	ReLU
Max pool	8 x 8 x 128	
4 x Convolutional	8 x 8 x 256	ReLU
Max pool	4 x 4 x 256	
4 x Convolutional	4 x 4 x 512	ReLU
Max pool	2 x 2 x 512	
4 x Convolutional	2 x 2 x 512	ReLU
Max pool	1 x 1 x 512	
Flatten		
FC	1024	ReLU
Dropout (0.3)		
FC	512	ReLU
Dropout (0.3)		
FC	64	ReLU
FC	10	Softmax

(b) CIFAR-10

Layer	Output shape	Activation function
Input	224 x 224 x 3	
7 x 7, 64, / 2	112 x 112 x 64	ReLU
3 x 3 max pool, / 2	56 x 56 x 64	
$\begin{bmatrix} 1 \times 1, 64 \\ 3 \times 3, 64 \\ 1 \times 1, 256 \end{bmatrix}$ x 3	56 x 56 x 64	ReLU
$\begin{bmatrix} 1 \times 1, 128 \\ 3 \times 3, 128 \\ 1 \times 1, 512 \end{bmatrix}$ x 8	28 x 28 x 128	ReLU
$\begin{bmatrix} 1 \times 1, 256 \\ 3 \times 3, 256 \\ 1 \times 1, 1024 \end{bmatrix}$ x 36	14 x 14 x 256	ReLU
$\begin{bmatrix} 1 \times 1, 512 \\ 3 \times 3, 512 \\ 1 \times 1, 2048 \end{bmatrix}$ x 3	7 x 7 x 512	ReLU
$\begin{bmatrix} 1 \times 1, 512 \\ 3 \times 3, 512 \\ 1 \times 1, 2048 \end{bmatrix}$ x 3	1 x 1 x 512	ReLU
Average pool	1 x 1 x 512	Softmax
Flatten		
FC	1024	ReLU
Dropout (0.3)		
FC	512	ReLU
FC	256	ReLU
FC	128	ReLU
FC	64	ReLU
FC	2	Softmax

(c) ImageNet

Table 2: The model architecture used for training each unlearnable dataset crafted by NTGA.

Layer	Output shape	Activation function
VGG19		
Flatten		
FC	2048	ReLU
Dropout (0.3)		
FC	1024	ReLU
Dropout (0.3)		
FC	512	ReLU
FC	256	ReLU
FC	128	ReLU
FC	64	ReLU
FC	10	Softmax

(a) Deepconfuse

Layer	Output shape	Activation function
Input	32 x 32 x 3	
2 x Convolutional	32 x 32 x 64	ReLU
Max pool	16 x 16 x 64	
2 x Convolutional	16 x 16 x 128	ReLU
Max pool	8 x 8 x 128	
3 x Convolutional	8 x 8 x 256	ReLU
Max pool	4 x 4 x 256	
3 x Convolutional	4 x 4 x 512	ReLU
Max pool	2 x 2 x 512	
3 x Convolutional	2 x 2 x 512	ReLU
Max pool	1 x 1 x 512	
Flatten		
FC	256	ReLU
FC	10	Softmax

(b) Error-minimizing

Layer	Output shape	Activation function
VGG16		
Flatten		
FC	2048	ReLU
FC	1024	ReLU
FC	512	ReLU
FC	256	ReLU
FC	180	ReLU
FC	128	ReLU
FC	64	ReLU
FC	10	Softmax

(c) Error-maximizing and REM

Layer	Output shape	Activation function
VGG19		
Flatten		
FC	1024	ReLU
FC	512	ReLU
FC	128	ReLU
FC	64	ReLU
FC	10	Softmax

(d) Synthetic, autoregressive, OPS, EnF, Hypocritical, and TensorClog

Table 3: The model architectures used for training the unlearnable CIFAR-10 images crafted by each approach.

5b illustrates the validation and training accuracy across epochs. Training the same model without

nonlinear transformations yielded a test accuracy of 39.24%, underscoring the substantial 49% accuracy

Protection approach	Nonlinear Transformations	Attributes for Keras ImageDataGenerator	Baseline model	Learning rate	# of epochs
NTGA	color channel manipulation (thrice)	rotation range of 7, zoom range of 0.3, width and height shift range of 0.35, horizontal flip, shear range of 0.4	VGG19	0.008	40
Deepconfuse	dilate, erode, and color channel manipulation (twice)	rotation range of 7, width shift range of 0.3, horizontal flip, zoom range of 0.1	VGG19	0.007	80
Error-minimizing	dilate, erode, color channel manipulation (twice), and Gaussian blur	rotation range of 7, height and width shift range of 0.3, horizontal flip, zoom range of 0.1	VGG16	0.006	80
Error-maximizing	dilate, erode, and color channel manipulation (twice)	rotation range of 10, shear range of 0.4, height and width shift range of 0.4, horizontal flip, zoom range of 0.4	VGG16	0.008	80
Synthetic	dilate, erode, and color channel manipulation (twice)	rotation range of 7, width and height shift range of 0.3, shear range of 0.4, horizontal flip, zoom range of 0.4	VGG19	0.007	40
Autoregressive	dilate, erode, and color channel manipulation (twice)	rotation range of 7, horizontal flip, zoom range of 0.1	VGG19	0.001	10
OPS	dilate, erode, and color channel manipulation (twice)	rotation range of 7, width and height shift range of 0.3, horizontal flip, zoom range of 0.1	VGG19	0.001	30
SEP	color channel manipulation (twice)	rotation range of 7, width and height shift range of 0.1, horizontal flip, zoom range of 0.1	VGG16	0.001	50
EntF	erode and color channel manipulation	rotation range of 7, width and height shift range of 0.3, horizontal flip, zoom range of 0.1	VGG19	0.001	30
REM	erode and color channel manipulation (twice)	rotation range of 7, width shift range of 0.15, and height shift range of 0.2, horizontal flip, zoom range of 0.1	VGG16	0.006	80
Hypocritical	dilate, erode and color channel manipulation	rotation range of 7, width and height shift range of 0.3, horizontal flip, zoom range of 0.1	VGG19	0.001	30
TensorClog	dilate, erode and color channel manipulation	rotation range of 7, width and height shift range of 0.3, horizontal flip, zoom range of 0.1	VGG19	0.001	30

Table 4: Summary of transformations and model specifications used to make these unlearnable CIFAR-10 images learnable.

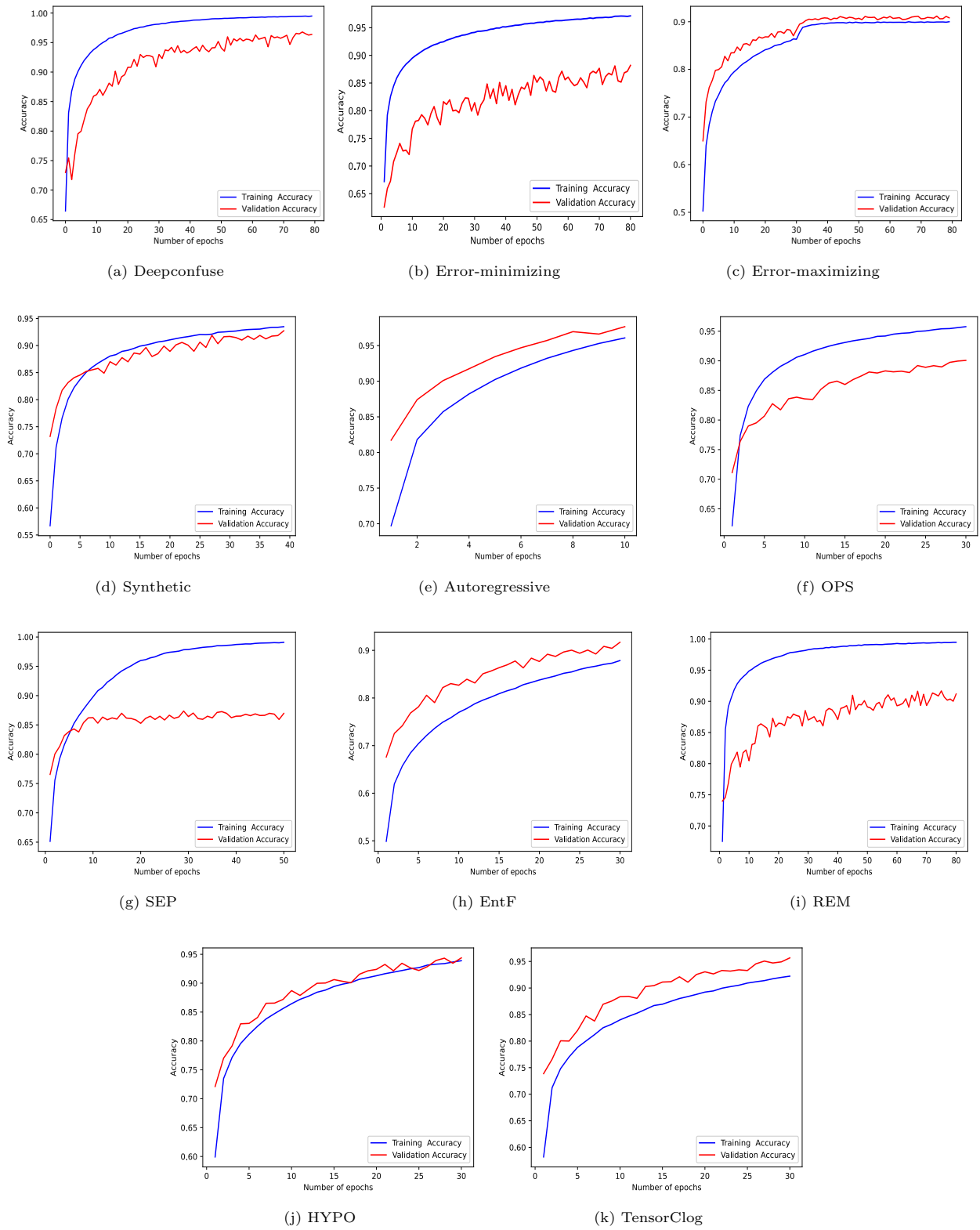


Figure 6: The training and validation accuracies of models trained with unlearnable CIFAR-10 crafted by other approaches.

improvement achieved through nonlinear transformations. Using the linear transformation technique in Segura et al. (2023) (OPA), we obtained a model with a test accuracy of 61.54%.

**Deepconfuse (Feng et al., 2019):** As reported in Feng et al. (2019), models trained on the CIFAR-10 unlearnable dataset generated by Deepconfuse exhibit an average test accuracy of 29%. To improve dataset learnability, we applied nonlinear transformations, such as dilate, erode, and color channel manipulation (applied twice), using a kernel size of 2 for dilation and erosion in the proposed framework. We further applied a built-in ImageDataGenerator from Keras with a rotation range of 7, a width shift range of 0.3, horizontal flip, and a zoom range of 0.1. The same ImageDataGenerator settings were used on the validation set. For the model architecture, we selected the VGG19 model as the baseline and added seven FC layers and two dropout layers, randomly dropping 30% of weights after the first two FC layers. The first FC layer had 2048 neurons, and subsequent layers halved the number of neurons until reaching 64. All FC layers (except the output layer) used ReLU as the activation function. The output layer, with softmax activation, comprised ten neurons. Table 3a provides an explicit display of this model architecture. The model was trained for 80 epochs with a learning rate of 0.007, achieving a test accuracy of 86.97%.

Training the same model without nonlinear transformations yielded a test accuracy of only 30.68%, consistent with the findings in Feng et al. (2019). Using OPA on the same dataset achieved a ResNet18 model with test accuracy of 75.28%. Hence, our nonlinear transformation approach yields a model that has a 15.57% improvement compared to the model trained with OPA. This result reaffirms that our approach can render unlearnable data learnable, showcasing the efficacy of nonlinear transformations.

**Error-minimizing (Huang et al., 2021):** To demonstrate the learnability of the unlearnable CIFAR-10 dataset generated by the error-minimizing approach, we augmented the dataset size to five times its original size using transformations detailed in Table 4. In addition to the nonlinear transformations applied to the Deepconfuse dataset, we included the Gaussian Blur transformation with a kernel size of 5 by 5. We also utilized the Keras ImageDataGenerator with settings similar to those for the Deepconfuse dataset, as outlined in Table 4 (with the addition of a height shift range

of 0.3). It is noteworthy that we exclusively employed the augmented dataset in this case, not the original unlearnable dataset. The baseline model for this experiment was VGG16, and the detailed model architecture is provided in Table 3b. Training the model for 80 epochs with a learning rate of 0.006 resulted in a test accuracy of 85.19%. However, utilizing the same model architecture without nonlinear transformation techniques led to a test accuracy of only 28.62%, akin to the result reported in Huang et al. (2021). Using OPA code on the same dataset, we achieved a model with test accuracy of 69.18%. Therefore, the model resulted using our approach showed 16.02% improvement in the test accuracy.

**Error-maximizing (Fowl et al., 2021):** According to the study Fowl et al. (2021), the lowest test accuracy of the model trained on the unlearnable CIFAR-10 data created by the error-maximizing approach is 6.25%. Our goal is to demonstrate that this dataset is still learnable by achieving a test accuracy of 85%. Table 4 shows that the nonlinear transformations used are similar to the ones for unlearnable CIFAR-10 images crafted by Deepconfuse. Table 3c presents the specifications of the model architecture used in this case. We chose the VGG16 model with pretrained ImageNet weights from the Keras Applications as the baseline model. Then, we added eight FC layers to the model. We trained the model for 80 epochs with a learning rate of 0.008, resulting in a test accuracy of 92.17%. The linear separable technique was only able to obtain a model with test accuracy of 75.57%.

**Synthetic (Yu et al., 2021):** The model trained on unlearnable CIFAR-10 examples crafted by the synthetic approach achieved a test accuracy of 13.54% reported in Yu et al. (2021). However, we demonstrate that these seemingly unlearnable CIFAR-10 examples from the synthetic approach are indeed learnable, achieving an 88% test accuracy with appropriate nonlinear transformations. Applying the same transformations used in the Deepconfuse and error-maximizing approaches, along with utilizing the built-in ImageDataGenerator from Keras on both the training and validation datasets, we trained the model with similar attributes as the error-minimizing approach (with the addition of a shear range of 0.4). The model architecture is detailed in Table 3d. Training the model for 40 epochs with a learning rate of 0.007 resulted in an 88.20% test accuracy, a 92.73% validation ac-

curacy, and a 93.48% training accuracy. Conversely, training the same model without nonlinear transformations led to a 42.7% test accuracy. Since the synthetic approach involves class-wise perturbations, the linear separability technique is reported to be effective in the breaking synthetic approach Segura et al. (2023). This fact is confirmed by the test accuracy of 87.9% we obtained after employing OPA.

**Autoregressive (Segura et al., 2022):** As per Segura et al. (2023), autoregressive perturbations are not linearly separable, making them difficult to break using OPA. In our experiments, we utilized an unlearnable dataset with autoregressive perturbation of  $\epsilon = 1$ , reported to have a test accuracy of 11.75%. Employing the same nonlinear transformations as Deepconfuse, error-maximizing, and synthetic approaches (summarized in Table 4), we also utilized the built-in ImageDataGenerator from Keras on the training and validation datasets with similar attributes to the error-minimizing approach, excluding height and width shift shear range. The model architecture employed is akin to the synthetic approach, as detailed in Table 3d. Training the model for ten epochs with a learning rate of 0.001, we achieved an 86.9% test accuracy, a 97.91% validation accuracy, and a 96.06% training accuracy. As expected, OPA was able to achieve a model with a low test accuracy of 25.59%.

**OPS (Wu et al., 2023):** As reported in Wu et al. (2023), the ResNet18 model trained on unlearnable examples generated by OPS perturbations achieved a test accuracy of 15.56%. Similar to synthetic perturbations, OPS is also a type of class-wise perturbations that is highly vulnerable to the linear transformation technique performed by OPA in Segura et al. (2023). Employing almost similar transformations as the autoregressive dataset, we used the same model architecture outlined in Table 3d. The model underwent training for 30 epochs with a learning rate of 0.001, resulting in a test accuracy of 86.71%. The ResNet18 model trained using OPA achieved a slightly better test accuracy of 88.10%, indicating that linear transformations are more appropriate for breaking OPS perturbations. Table 4 details the nonlinear transformations applied to this dataset. In addition to the techniques used for autoregressive perturbations, we introduced a width and height shift range of 0.3. The model achieved a training accuracy of 95.77% and a validation accuracy of 90.07%.

**SEP (Chen et al., 2022):** We tested the SEP data protection approach using our frame-

work. Employing their GitHub code, we generated the best-protected dataset, SEP-FA-VR, with a perturbation radius of 2/255. the VGG16 model (from the PyTorch code in their GitHub repository) trained on this dataset achieved a test accuracy of 24.88%, consistent with results in Chen et al. (2022). However, using TensorFlow’s pretrained VGG16 model with ImageNet weights on the same unlearnable dataset, without any transformations, we achieved a higher test accuracy of 83.81%. This highlights the enhancing effect of pretrained models on learning from SEP-protected data. Further applying our nonlinear transformations approach boosted the test accuracy to 88.81%. It is worth noticing that OPA also achieved a model with almost the same test accuracy of 87.28%. In this instance, we used color channel manipulation twice to expand the training dataset, along with the built-in ImageDataGenerator from Keras, incorporating a rotation range of 7, width and height shift range of 0.1, horizontal flip, and a zoom range of 0.1.

**EntF (Wen et al., 2023):** EntF is a recently proposed data protection approach created using entangled features. We generated unlearnable CIFAR-10 dataset perturbed with EntF by employing their code on GitHub with default settings (perturbation radius of 8/255). As per Wen et al. (2023), an adversarially trained model on an unlearnable dataset achieved a test accuracy of 71.57%. Our aim, using the outlined approach, was to reach a model with an 85% accuracy. Employing the VGG19 model described in Table 3d initialized with ImageNet weights, we expanded the training dataset twice using erode and color channel manipulation. Additionally, we applied the built-in ImageDataGenerator from Keras with a rotation range of 7, width and height shift range of 0.3, horizontal flip, and a zoom range of 0.1. After 30 epochs of training, the model achieved a test accuracy of 88.59%. The training and validation accuracies of the model are 87.85% and 95.39%, respectively. After applying OPA on the same dataset, we obtained a model with test accuracy of 85.67%. Hence, our approach shows 3.41% improvement compared to OPA.

**REM (Fu et al., 2022):** The CIFAR-10 dataset with REM noise is generated using their GitHub code with default settings (perturbation radius of 4/255). As reported in Fu et al. (2022), the model trained on this dataset achieved a test accuracy of 27.09%. To transform the unlearnable dataset, we applied color channel manipulation twice and

an erode. Additionally, we utilized Keras ImageDataGenerator with a zoom range of 0.1, a rotation range of 7, a width shift range of 0.15, a height shift range of 0.2, and a horizontal flip. Training with the same model architecture as presented in Table 3c but excluding the fully connected layer with 180 neurons, we trained for 80 epochs with a learning rate of 0.006, resulting in a test accuracy of 85.70%. This demonstrates the model’s ability to learn from the ostensibly unlearnable data with REM noise. We then applied OPA on the dataset but obtained a lower test accuracy of 34.78%, meaning that REM perturbations are not vulnerable to linear transformations. This fact is confirmed by the similar results in Segura et al. (2023). Hence, our nonlinear approach obtained a model with 50.92% more accuracy than the model obtained using the linear approach. However, the model exhibits a training accuracy of 99.47% and a validation accuracy of 93.88%.

**Hypocritical (Tao et al., 2021):** Hypocritical perturbations is one of the data protection approaches discussed in Tao et al. (2021). We generated the class-wise Hypocritical perturbations since it is more effective than sample-wise perturbations. After applying the standard training method provided in their GitHub repository on the generated unlearnable CIFAR-10 dataset, the resulting model achieved a test accuracy of 18.59%, consistent with the result reported in Tao et al. (2021). However, using the pretrained model in Table 3d without any transformations on the same dataset, we obtained a test accuracy of 79.77%. Employing similar settings, including model specification and transformations techniques as One-Pixel Shortcut on the Hypocritical perturbations (Tao et al., 2021), with the only difference of using color channel manipulation only once, not twice, we achieved a test accuracy of 89.68%. The training and validation accuracies are 93.89% and 94.38%, respectively, indicating that Hypocritical perturbations are vulnerable to our approach. After applying OPA, we obtained a model with a test accuracy of 86.79%. It is reasonable that this dataset can be broken by the orthogonal projection method since it has class-wise perturbations.

**TensorClog (Shen et al., 2019):** According to Shen et al. (2019), TensorClog perturbations can reduce the test accuracy of a model trained on CIFAR-10 from 86.05% (based on clean data) to 48.07%. We generated the CIFAR-10 dataset with TensorClog perturbations using default set-

tings from their GitHub repository. Training the model in Table 3d on this dataset without our approach resulted in a test accuracy of 83.53%. However, with our approach-expanding the training set threefold using dilate, erode, and color channel manipulation, and applying Keras ImageDataGenerator with attributes from Table 4-the model’s test accuracy notably increased to 89.68%. These findings highlight the effectiveness of our approach in handling unlearnable data with TensorClog perturbations. However, OPA also resulted in a model with almost similar test accuracy of 88.05%, showing that TensorClog perturbations are vulnerable to linear transformations.

#### 4.2. Comparison with Adversarial Training

To demonstrate our approach’s effectiveness, we compared it with adversarial training, a prominent defense mechanism (Fu et al., 2022; Tao et al., 2022). Following Fu et al. (2022)’s approach, we conducted adversarial training using PGD attack (Madry et al., 2018) with VGG19 and VGG16 as base models, ensuring compatibility with our architectures. Perturbation radius and step-size were set to 4/255 and 0.8/255 (default), respectively, for all unlearnable noises, except error-minimizing noise. For the latter, a perturbation radius of 8/255 and step-size of 2/255 were used, resulting in better accuracy than a perturbation radius of 4/255. Default values were maintained for other parameters, such as 10 PGD steps and 40000 training iterations. Test accuracies under adversarial training are reported in Column 7 in Table 1, showcasing our approach’s superiority across all considered noises.

#### 4.3. Perturbed 50% of the Training Set

In our experiments, we also consider the case in which only 50% of the dataset is unlearnable. Similar to the experiment in Section 4.1, we performed on the CIFAR-10 crafted by Deepconfuse, error-minimizing, error-maximizing, synthetic, autoregressive, OPS, SEP, Entangled Features, REM, Hypocritical, and TensorClog approaches, respectively. We did not perform any nonlinear transformations for the training set and used similar models in Table 3a-3d. The models achieved a test accuracy of 85.65%, 86.28%, 86.49%, 83.8%, 87.56%, 86.69%, 87.81%, 86.72%, 86.73%, 88.53%, and 86.14%, respectively. This also demonstrates the limited effectiveness of those data protection approaches. That is, these approaches are vulnerable to nonlinear transformations and ineffective when only half of the dataset is protected.

#### 4.4. Our Proposed Approach with A Series of Transformations

In Section 4.1, we only applied each nonlinear transformation technique directly on the unlearnable datasets generated by the aforementioned data protection approaches without considering the effectiveness of the series of transformations, e.g., applying pixel manipulation on a dilated image instead of the original image. In this section, we present experimental results obtained using a series of transformations for a single unlearnable input image.

The first four steps of the series of transformations are the same for all four unlearnable datasets. (1). We randomly selected an angle between 0 and 22.5 degrees and rotate the input image by the chosen angle. (2). We cropped the image to trim away the outer edges. The amount trimmed away is randomly determined to be between 0 and 5 pixels from the edge. (3). Since the model requires a fixed image size, we resized the image to 32x32x3 using cubic interpolation in `cv2.resize` function. (4). We flipped the image horizontally with a 50/50 chance. The next few transformations vary depending on the data protection approach. However, we always converted the image to a grayscale at the end of the series, irrespective of the dataset.

**NTGA (Yuan and Wu, 2021):** We increased contrast and brightness by 50%, and saturation by 100% with a probability of 0.5 in order. Then, we changed the hue with a probability of 0.8 and converted the image to grayscale with a probability of 0.9. We expanded the training dataset five times by repeating this series of transformations on each image. Using the expanded training dataset, we trained the model presented in Table 3c for 80 epochs. Based on the trained model, we obtained a test accuracy of 83.81%.

**Deepconfuse (Feng et al., 2019):** For the Deepconfuse CIFAR-10 dataset, with a probability of 0.8, we changed the hue using `cv2.COLOR_HSV2RGB` function. Finally, with a probability of 0.8, we converted the image into a grayscale one using `cv2.COLOR_BGR2GRAY` function. Repeatedly applying this series of transformations five times to increase the training set size. For the resulting training set, we made a few changes to the training model in Table 3a, i.e., changing the dropout rate to 60% for the first dropout layer and adding the FC layer with 32 neurons to achieve the test accuracy of 85.51%. This indicates that the model can still learn from protected data.

**Error-minimizing (Huang et al., 2021):** Instead of changing hue, we manipulated the brightness and contrast of the error-minimizing CIFAR-10 dataset. With a probability of 0.2, we increased the contrast of each image by 50%. Similarly, with a probability of 0.2, we increased the brightness by 50%. We used `ImageEnhance` function in Python Pillow to manipulate brightness and contrast. Finally, we converted the image to grayscale with a probability of 0.95. Repeating this series of textcolorednonlinear transformations six times, we reached 85.34% test accuracy using the same model architecture as in Table 3b.

**Error-maximizing (Fowl et al., 2021):** The transformations series steps we used for the error-maximizing CIFAR-10 dataset are almost identical to the one used for the error-minimizing CIFAR-10 dataset but with one extra step, namely, changing the saturation of the image. However, we applied each of these techniques with a probability of 0.8. Using the same model architecture as in Table 3c, we achieved a test accuracy of 86.18%.

**Synthetic (Yu et al., 2021):** For the synthetic CIFAR-10 dataset, after common initial steps of transformation techniques, we increased the image’s brightness by 50% with a applying probability of 0.5. Finally, with a probability of 0.9, we changed the image to grayscale. Then, we repeatedly applied this series of transformations five times to increase the training set size for the subsequence training and chose the same model architecture as the one displayed in Table 3d. Furthermore, we added a dropout layer with a dropout rate of 50% after the flattened layer. In the end, we achieved a test accuracy of 83.59%, again indicating that the model is learning from “unlearnable” data.

**Autoregressive (Segura et al., 2022):** We applied the same transformations used in the error-minimizing approach to the autoregressive-generated CIFAR-10 dataset. Specifically, we expanded the training set five times as the original size and used the model in Fig. 3d for training. After training the model for five epochs, we achieved a test accuracy of 85.73%.

**SEP (Chen et al., 2022):** For the dataset created with SEP perturbations, we applied a almost the same series of transformations used in the error-minimizing approach. We adjusted contrast and brightness with probabilities of 0.5 and 0.2, respectively. Then, we used grayscale with a probability of 0.8 and expanded the training set four times. Utilizing VGG16 with an additional fully connected

layer comprising ten neurons allowed us to integrate outputs, resulting in a test accuracy of 86.53%.

**EntF (Wen et al., 2023):** In our experiment, we replicated the same series of transformations as SEP on the dataset protected by EntF but adjusted the grayscale probability to 0.9. Furthermore, our model architecture was also chosen as the same one used in the SEP approach, i.e., the VGG16 model with an one additional layer having ten neurons. After we applied the series of transformations, the training set was expanded four times. This setup resulted in a test accuracy of 86.33%.

**REM (Fu et al., 2022):** For the unlearnable dataset created with REM perturbations, we applied the same series of transformation used on the unlearnable dataset with EntF noise. Moreover, we utilized the same model architecture as the one used in the SEP approach and increased the size of the training dataset six times before training. The model was trained for 60 epochs with a learning rate of 0.006. Our experiment achieved a test accuracy of 83.19%.

**Hypocritical (Tao et al., 2021):** For the CIFAR-10 dataset with Hypocritical perturbations, we modified contrast, brightness, and saturation in order with a probability of 0.5, and grayscale with probability of 0.9. The model architecture for our experiment was VGG19 with two additional FC layers of 256 and ten neurons. We expanded the training set five times incorporating the aforementioned series of transformations, which results in a model that achieves a test accuracy of 86.30%.

**OPS (Wu et al., 2023):** In our experiment, a series of transformations did not perform well on the One-Pixel Shortcut dataset initially. After modifying contrast, brightness, saturation with a probability of 0.5 and grayscale with a probability of 0.9. Unlike in other datasets, we used a built-in Imagedatagenerator with a rotation range of 7, a width and height shift range of 0.1, a horizontal flip, and a zoom range of 0.1 to achieve this accuracy. Our experiment achieved a test accuracy of 79.32% only.

**TensorClog (Shen et al., 2019):** In our experiment, the series of transformations used for the unlearnable CIFAR-10 dataset with tensorClog perturbations are contrast, brightness, and grayscale with a probability of 0.5, 0.2, and 0.9 respectively. The model architecture used is provided in Table 3d, resulting in a model that achieves a test accuracy of 86.53%.

## 5. Discussion

Section 4 provides an evaluation of twelve data protection approaches, revealing their vulnerability to nonlinear transformations and the subsequent degradation of protection levels. Figures 5 and 6 illustrate that validation accuracy curves, in contrast to their corresponding training curves, exhibit some degree of overfitting for specific unlearnable datasets. This suggests that our approach facilitates the transformation of unlearnable data into learnable, albeit with potential disparities in the distributions of training and validation data.

In this section, we discuss additional experimental results. To evaluate the effectiveness of our approach on diverse datasets, we experimented on unlearnable MNIST and ImageNet datasets crafted by the NTGA. We also present an experimental evaluation for an additional data protection approach, CUDA (Sadasivan et al., 2023a). Recent studies in Liu et al. (2023); Qin et al. (2023); Segura et al. (2023) have delved into approaches for breaking unlearnable datasets. We provide a comprehensive discussion outlining the distinctions between our approach and theirs.

**NTGA on MNIST:** As shown in Yuan and Wu (2021), the lowest test accuracy of the model trained based on unlearnable MNIST dataset is around 16% for Convolutional Neural Networks (CNNs). Our objective is to demonstrate that these so-called “unlearnable data” can achieve a test accuracy of 98%, matching the performance of a model trained on clean data. In essence, we elevate the test accuracy from 16% to 98% through image transformation techniques outlined in Section 3.3. Initially, we employed image nonlinear transformation methods to render unlearnable data learnable, utilizing the Keras ImageDataGenerator function with attributes like a rotation range of 10 and a zoom range of 0.1. Subsequently, we applied the threshold binary transformation with a threshold value of 0.5 and a maximum value of 1 to the training dataset. Lastly, we utilized the JPEG Compression transformation. Table 2a shows the model used for this experiment. The model consists of two convolution layers with ReLU activation function and two fully connected (FC) layers. The first FC layer has 1024 units with an ReLU activation function, and the next one has ten units with the softmax activation function. In addition, a dropout layer is added between the two FC layers that randomly drops 25% of the weights. The model was trained for ten epochs with a batch size

of 100. This setup gave a test accuracy of 98.9%, the same as the accuracy obtained based on clean data. In contrast, employing the same model architecture without nonlinear transformations resulted in a mere test accuracy of 17.50%. This showcases the vulnerability of the unlearnable MNIST dataset crafted by NTGA to the effects of data augmentation. Fig. 5a illustrates the training and validation accuracy evolution.

**NTGA on ImageNet:** The test accuracy remains around 70% for most model architectures in Yuan and Wu’s study on their unlearnable ImageNet dataset (Yuan and Wu, 2021). We performed the proposed framework using the Keras ImageDataGenerator by setting the rotation range to 2, the horizontal flip to True, and the zoom range to 0.1. Moreover, the training dataset was increased up to three times the original dataset size using nonlinear transformations in the OpenCV package. These nonlinear transformations are color channel manipulation, thresh binary, and thresh binary inverse, with a threshold value of 0.5 and a maximum value of 1.

The baseline model we used for this experiment is ResNet with 152 convolution layers (ResNet152) and random initialization of weights. We extended the model by adding six FC layers and one dropout layer after a series of convolutional layers from ResNet152. These FC layers have 1024, 512, 256, 128, and 64 units with an ReLU activation function. The last layer has two neurons with a softmax activation function. Furthermore, we added a dropout layer after the first layer, which will lead to a 30% random drop of the model weights. Table 2c provides the details of the specifications of the model architecture. We trained the model for 100 epochs with a batch size of 10 and a learning rate of 0.001. This setup yielded a training accuracy of 99.36%, a validation accuracy of 95.26%, and a test accuracy of 95.71%. The test accuracy closely matches models trained on clean data, underscoring the vulnerability of NTGA to our approach. Fig. 5c depicts the validation and training accuracy throughout the model training process. Employing the same model architecture without our framework yielded a test accuracy of only 75.71%. This outcome underscores the significant impact of nonlinear transformations on the success or failure of data protection approaches, such as NTGA in the above experiments.

**CUDA (Sadasivan et al., 2023a):** As proposed by Sadasivan et al. (2023a), we generated

a Convolution-based Unlearnable Dataset (CUDA) using the code provided in their Git-Hub repository. We used a blur parameter of 0.3 to obtain a dataset with enhanced protection. Initially, when a VGG16 model was trained on these images, the test accuracy was only 10.56%. However, by expanding the training dataset through cropping and dilating techniques and incorporating the Keras ImageDataGenerator, we achieved a significantly improved test accuracy of 43.35%. Unlike other approaches, such as error-minimizing, error-maximizing, and NTGA, CUDA is not model-dependent and does not produce additive noises. CUDA introduces multiplicative noise, resulting in more noise in the image’s background. As most of the noise in this dataset is in the background, we noticed that cropping the background is effective.

Moreover, we applied a series of transformations to the CUDA dataset. Initially, we cropped 1 pixel from each side of the borders. Then, we implemented a horizontal flip with a probability of 0.5. Contrast and brightness were increased by 50% with a probability of 0.7. Next, we increased saturation and sharpness to twice their existing values with a probability of 0.7. We further added a contour filter with a probability of 0.2 and increased the hue channel by 10. For images that did not have a contour filter added, we used a posterize filter with a probability of 0.7. Finally, we applied grayscale with a probability of 0.2. Training these transformed unlearnable images on the model shown in Table 3c without the first fully connected layer with 2048 neurons achieved a test accuracy of 77.36%. However, the model’s training and validation accuracies were 81.22% and 97.71%, respectively. Additionally, further exploration of more advanced and specified transformations is necessary to break the CUDA-protected dataset, especially considering CUDA’s significant difference in methodology from other approaches.

**UEraser (Qin et al., 2023)** is a recently proposed approach to break unlearnable data. In contrast to our approach, they utilized modern image transformation techniques such as PlasmaTransform and ChannelShuffle. Initially, we replicated their experiments using the code in their GitHub repository. UEraser is applied on the unlearnable CIFAR-10 dataset with synthetic perturbation, which resulted in a test accuracy of 91.97%. We executed the code without UEraser, and the test accuracy is 19.95%. Then, we replaced the modern image transformation in UEraser with the

nonlinear transformation techniques we used. They are rotate, resize, flip, brightness, and grayscale. This modification led to a test accuracy of 88.97%. This demonstrates that despite their use of modern image transformation techniques, our approach remains almost as effective as UEraser.

Furthermore, the following work is also related to our research.

**Image Shortcut Squeezing (ISS) (Liu et al., 2023)** explored an attack method against unlearnable data based on simple compression techniques. They mainly used grayscale and compression methods, such as JPEG compression, to mitigate the effect of unlearnability. Their main focus was on evaluating the effectiveness of image squeezing methods against unlearnable data, while our study concentrates on a broader area, including nonlinear transformations and building a framework to overcome unlearnability. ISS was able to improve CIFAR-10 model accuracy to 81.73% for twelve existing unlearnable methods. We successfully assessed the same eleven approaches, and achieved a test accuracy exceeding 85%, including the EntF approach (Wen et al., 2023), which they had not explored. The ShortcutGen dataset (van Vlijmen et al., 2022) is the only approach we did not consider because the code is not publicly available.

## 6. Conclusion

Recent advancements in defense mechanisms, such as NTGA and Deepconfuse, aim to safeguard data against unauthorized deep learning use. However, our research exposed vulnerabilities in these approaches, particularly when confronted by the proposed nonlinear transformation framework. Testing on CIFAR-10, ImageNet, and MNIST datasets revealed that data assumed to be unlearnable could achieve over 85% accuracy through our proposed nonlinear transformation techniques, compromising the efficacy of existing data protection measures. Our approach provides a model with improved test accuracy than the existing linear separable approach given in Segura et al. (2023) on eleven CIFAR10 datasets. This highlights a significant gap in current defense methods, as even partial clean datasets exhibit high accuracy. Our findings underscore the importance of exploring more effective data protection approaches and developing robust data protection approaches capable of withstanding such techniques. This emphasizes the necessity of considering nonlinear transformations in the future development of resilient data protection approaches.

## 7. Appendix

### 7.1. Visualization of Unlearnable Examples

In this study, we have explored twelve well-known data protection approaches. In this section, we provide a visualization of examples from each dataset. Fig. 7 shows the unlearnable examples crafted by NTGA. Those were acquired from Kaggle, where the authors publicly released those unlearnable examples. The unlearnable MNIST training dataset includes 50,000 images that were classified into ten classes, as shown in Fig. 7a. The resolution of the images is 28 x 28 x 1. The test dataset includes 10,000 images, whereas the validation dataset also contains 10,000 images. The unlearnable CIFAR-10 dataset crafted by NTGA has 40,000 poisoned images, the validation set has 10,000 clean images, and the test dataset has 10,000 unseen clean images. The images are classified into ten classes, and the image resolution is 32 x 32 x 3. Fig. 7b illustrate these unlearnable CIFAR-10 data. ImageNet data have a higher resolution than CIFAR-10 with 224 x 224 x 3 pixels. Similar to Yuan and Wu (2021), we only consider the “bulbul” and “jellyfish” classes. Fig. 7c provides a visualization of these data. The training dataset has 2,220 unlearnable images, the validation dataset has 380 images, and the testing dataset has 100 images.

### 7.2. A List of GitHub Source Codes

In our research, the datasets generated by Deepconfuse, error-minimizing, error-maximizing, and synthetic approaches were obtained from Yu et al. (2021). The datasets created by other approaches—autoregressive, OPS, SEP, EntF, REM, Hypocritical, and TensorClog were generated using the available code in their respective GitHub repositories. The links for GitHub repositories are provided in Table 5.

## References

- Agarap, A.F., 2018. Deep learning using rectified linear units (ReLU). CoRR abs/1803.08375. [arXiv:1803.08375](https://arxiv.org/abs/1803.08375).
- Chaumette, F., Marchand, E., Melchior, N., Saunier, A., Spindler, F., Tallonneau, R., 2012. Image manipulation and processing. ViSP tutorial, Lagadic project .
- Chen, F., Ma, J., 2009. An empirical identification method of gaussian blur parameter for image deblurring. *IEEE Trans. Signal Process.* 57, 2467–2478. doi:10.1109/TSP.2009.2018358.
- Chen, S., Yuan, G., Cheng, X., Gong, Y., Qin, M., Wang, Y., Huang, X., 2022. Self-ensemble protection: Training checkpoints are good data protectors. *arXiv preprint arXiv:2211.12005* .
- Dao, T., Gu, A., Ratner, A., Smith, V., De Sa, C., Ré, C., 2019. A kernel theory of modern data augmentation, in: *International Conference on Machine Learning*, PMLR. pp. 1528–1537.

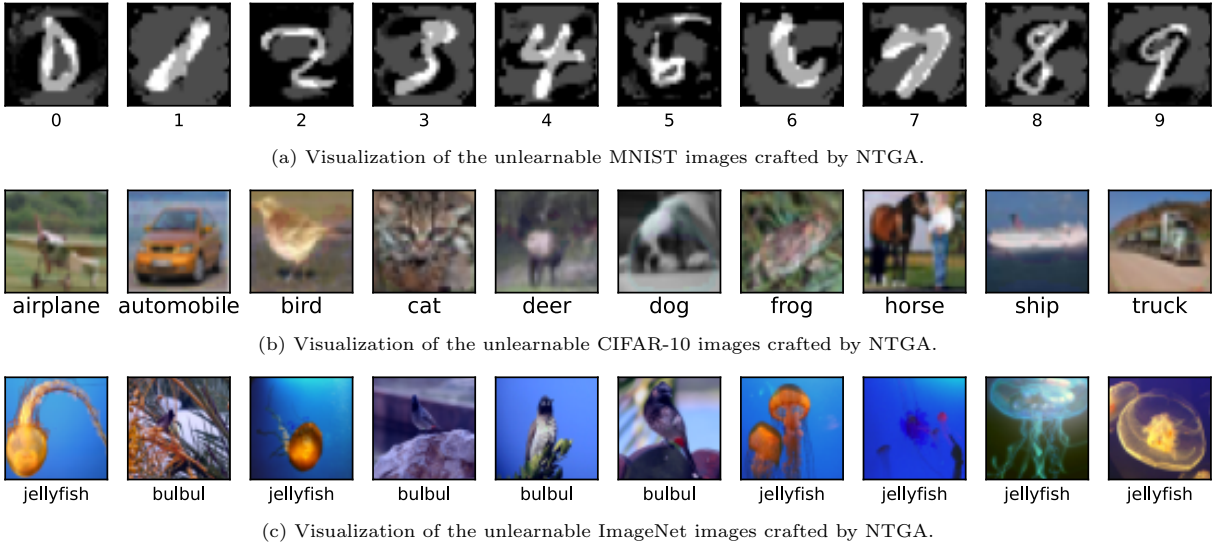


Figure 7: Unlearnable MNIST, CIFAR-10, and ImageNet examples generated by NTGA.

Protection approach	Source code
NTGA	<a href="https://github.com/lionelmessi6410/ntga?tab=readme-ov-file#unlearnable-datasets">https://github.com/lionelmessi6410/ntga?tab=readme-ov-file#unlearnable-datasets</a>
Autoregressive	<a href="https://github.com/psandovalsegura/autoregressive-poisoning">https://github.com/psandovalsegura/autoregressive-poisoning</a>
OPS	<a href="https://github.com/cycomatica/One-Pixel-Shotcut">https://github.com/cycomatica/One-Pixel-Shotcut</a>
SEP	<a href="https://github.com/Sizhe-Chen/SEP">https://github.com/Sizhe-Chen/SEP</a>
EntF	<a href="https://github.com/WenRuiUSTC/EntF">https://github.com/WenRuiUSTC/EntF</a>
REM	<a href="https://github.com/fshp971/robust-unlearnable-examples">https://github.com/fshp971/robust-unlearnable-examples</a>
Hypocritical	<a href="https://github.com/TLMichael/Delusive-Adversary/tree/main">https://github.com/TLMichael/Delusive-Adversary/tree/main</a>
TensorClog	<a href="https://github.com/JC-S/TensorClog_Public">https://github.com/JC-S/TensorClog_Public</a>

Table 5: List of GitHub source codes.

- Deng, J., Dong, W., Socher, R., Li, L., Li, K., Fei-Fei, L., 2009. Imagenet: A large-scale hierarchical image database, in: IEEE Computer Society Conference on Computer Vision and Pattern Recognition (CVPR) Miami, Florida, USA, IEEE Computer Society. pp. 248–255. doi:10.1109/CVPR.2009.5206848.
- Feng, J., Cai, Q., Zhou, Z., 2019. Learning to confuse: Generating training time adversarial data with auto-encoder, in: Wallach, H.M., Larochelle, H., Beygelzimer, A., d’Alché-Buc, F., Fox, E.B., Garnett, R. (Eds.), Advances in Neural Information Processing Systems 32: Annual Conference on Neural Information Processing Systems (NeurIPS), Vancouver, BC, Canada, pp. 11971–11981.
- Fowl, L., Goldblum, M., Chiang, P., Geiping, J., Czaja, W., Goldstein, T., 2021. Adversarial examples make strong poisons, in: Ranzato, M., Beygelzimer, A., Dauphin, Y.N., Liang, P., Vaughan, J.W. (Eds.), Advances in Neural Information Processing Systems 34: Annual Conference on Neural Information Processing Systems (NeurIPS), virtual, pp. 30339–30351.
- Fu, S., He, F., Liu, Y., Shen, L., Tao, D., 2022. Robust unlearnable examples: Protecting data privacy against adversarial learning, in: The Tenth International Conference on Learning Representations (ICLR), OpenReview.net.
- Gervasi, O., Caprini, L., Maccherani, G., 2013. Virtual exhibitions on the web: From a 2d map to the virtual world, in: Murgante, B., Misra, S., Carlini, M., Torre, C.M., Nguyen, H., Taniar, D., Apduhan, B.O., Gervasi, O. (Eds.), Computational Science and Its Applications (ICCSA), Ho Chi Minh City, Vietnam, Springer. pp. 708–722. doi:10.1007/978-3-642-39637-3\\_56.
- Gonzalez, R.C., Woods, R.E., 2008. Digital image processing. Prentice Hall, Upper Saddle River, N.J.
- Haralick, R.M., Sternberg, S.R., Zhuang, X., 1987. Image analysis using mathematical morphology. IEEE Trans. Pattern Anal. Mach. Intell. 9, 532–550. doi:10.1109/TPAMI.1987.4767941.
- Harris, E., Marcu, A., Painter, M., Niranjana, M., Prügel-Bennett, A., Hare, J., 2020a. Fmix: Enhancing mixed sample data augmentation. arXiv preprint arXiv:2002.12047 .
- Harris, E., Marcu, A., Painter, M., Niranjana, M., Prügel-Bennett, A., Hare, J.S., 2020b. Understanding and enhancing mixed sample data augmentation. CoRR abs/2002.12047. arXiv:2002.12047.
- He, H., Zha, K., Katabi, D., 2022. Indiscriminate poisoning attacks on unsupervised contrastive learning. CoRR abs/2202.11202. arXiv:2202.11202.
- Huang, H., Ma, X., Erfani, S.M., Bailey, J., Wang, Y., 2021. Unlearnable examples: Making personal data unexploitable, in: 9th International Conference on Learning Representations (ICLR), Virtual Event, Austria, OpenReview.net.
- Jacot, A., Hongler, C., Gabriel, F., 2018. Neural tangent kernel: Convergence and generalization in neural net-



(a) Deepconfuse.



(b) Error-minimizing.



(c) Error-maximizing.



(d) Synthetic.



(e) Autoregressive.



(f) OPS.



(g) SEP.



(h) EntF.

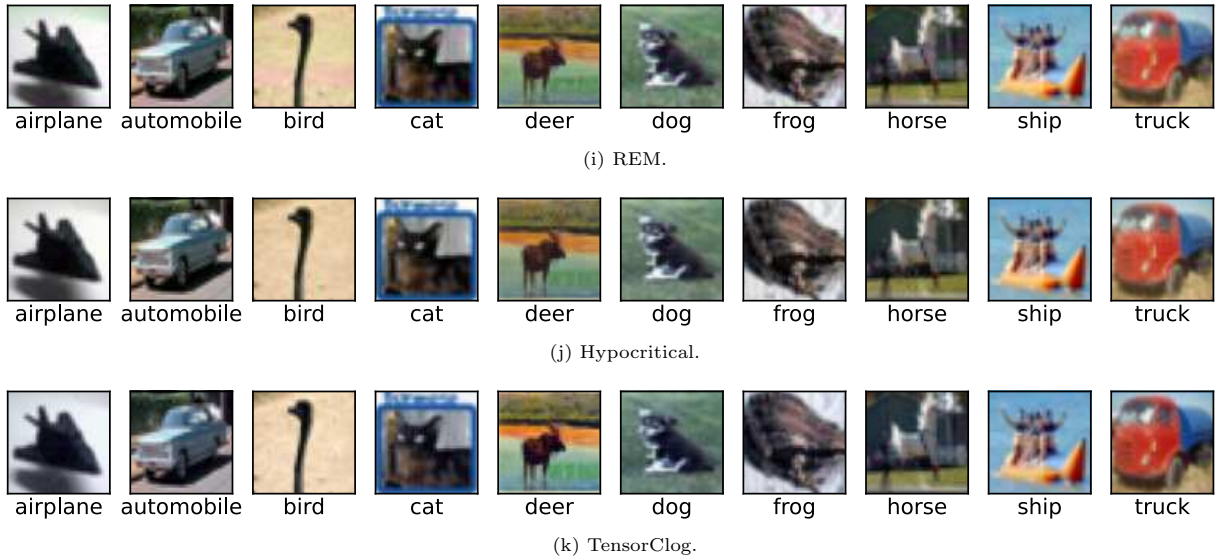


Figure 8: Visualization of the unlearnable CIFAR-10 images crafted by the other eleven approaches.

- works, in: Bengio, S., Wallach, H.M., Larochelle, H., Grauman, K., Cesa-Bianchi, N., Garnett, R. (Eds.), *Advances in Neural Information Processing Systems 31: Annual Conference on Neural Information Processing Systems (NeurIPS)*, Montréal, Canada, pp. 8580–8589.
- Jagielski, M., Oprea, A., Biggio, B., Liu, C., Nita-Rotaru, C., Li, B., 2018. Manipulating machine learning: Poisoning attacks and countermeasures for regression learning, in: *IEEE Symposium on Security and Privacy (S&P)*, IEEE. pp. 19–35.
- Koh, P.W., Liang, P., 2017. Understanding black-box predictions via influence functions, in: *International conference on machine learning*, PMLR. pp. 1885–1894.
- Komarudin, A., Satria, A.T., Atmadja, W., 2015. Designing license plate identification through digital images with opencv. *Procedia Computer Science* 59, 468–472.
- Krizhevsky, A., Hinton, G., et al., 2009. Learning multiple layers of features from tiny images. Technical report .
- LeCun, Y., Cortes, C., 2010. MNIST handwritten digit database. ATT Labs .
- Liu, Z., Zhao, Z., Larson, M., 2023. Image shortcut squeezing: Countering perturbative availability poisons with compression. *arXiv preprint arXiv:2301.13838* .
- Madry, A., Makelov, A., Schmidt, L., Tsipras, D., Vladu, A., 2018. Towards deep learning models resistant to adversarial attacks, in: *6th International Conference on Learning Representations (ICLR)*, Vancouver, BC, Canada, Conference Track Proceedings, OpenReview.net.
- Qin, T., Gao, X., Zhao, J., Ye, K., Xu, C.Z., 2023. Learning the unlearnable: Adversarial augmentations suppress unlearnable example attacks. *arXiv preprint arXiv:2303.15127* .
- Qiu, H., Zeng, Y., Guo, S., Zhang, T., Qiu, M., Thuringham, B., 2021. Deepsweep: An evaluation framework for mitigating DNN backdoor attacks using data augmentation, in: *Proceedings of the ACM Asia Conference on Computer and Communications Security*, pp. 363–377.
- Rahmatullah, P., Abidin, T.F., Misbullah, A., et al., 2021. Effectiveness of data augmentation in multi-class face recognition, in: *2021 5th International Conference on Informatics and Computational Sciences (ICICoS)*, IEEE. pp. 64–68.
- Sadasivan, V.S., Soltanolkotabi, M., Feizi, S., 2023a. Cuda: Convolution-based unlearnable datasets, in: *Proceedings of the IEEE/CVF Conference on Computer Vision and Pattern Recognition*, pp. 3862–3871.
- Sadasivan, V.S., Soltanolkotabi, M., Feizi, S., 2023b. FUN: Filter-based unlearnable datasets.
- Segura, P.S., Singla, V., Geiping, J., Goldblum, M., Goldstein, T., 2023. What can we learn from unlearnable datasets?, in: Oh, A., Naumann, T., Globerson, A., Saenko, K., Hardt, M., Levine, S. (Eds.), *Advances in Neural Information Processing Systems 36: Annual Conference on Neural Information Processing Systems 2023, NeurIPS 2023, New Orleans, LA, USA, December 10 - 16, 2023*. URL: [http://papers.nips.cc/paper\\_files/paper/2023/hash/ee5bb72130c332c3d4bf8d231e617506-Abstract-Conference.html](http://papers.nips.cc/paper_files/paper/2023/hash/ee5bb72130c332c3d4bf8d231e617506-Abstract-Conference.html).
- Segura, P.S., Singla, V., Geiping, J., Goldblum, M., Goldstein, T., Jacobs, D.W., 2022. Autoregressive perturbations for data poisoning. *CoRR abs/2206.03693*. doi:10.48550/arXiv.2206.03693, *arXiv:2206.03693*.
- Shen, J., Zhu, X., Ma, D., 2019. Tensorclog: An imperceptible poisoning attack on deep neural network applications. *IEEE Access* 7, 41498–41506. URL: <https://doi.org/10.1109/ACCESS.2019.2905915>, doi:10.1109/ACCESS.2019.2905915.
- Shokri, R., Stronati, M., Song, C., Shmatikov, V., 2017. Membership inference attacks against machine learning models, in: *IEEE Symposium on Security and Privacy (SP)*, San Jose, CA, USA, IEEE Computer Society. pp. 3–18. doi:10.1109/SP.2017.41.
- Simonyan, K., Zisserman, A., 2015. Very deep convolutional networks for large-scale image recognition, in: Bengio, Y., LeCun, Y. (Eds.), *3rd International Conference on Learning Representations (ICLR)*, San Diego, CA, USA, Con-

- ference Track Proceedings.
- Srivastava, N., Hinton, G., Krizhevsky, A., Sutskever, I., Salakhutdinov, R., 2014. Dropout: a simple way to prevent neural networks from overfitting. *The journal of machine learning research* 15, 1929–1958.
- Tao, L., Feng, L., Wei, H., Yi, J., Huang, S., Chen, S., 2022. Can adversarial training be manipulated by non-robust features?, in: *NeurIPS*. URL: [http://papers.nips.cc/paper\\_files/paper/2022/hash/a94a8800a4b0af45600bab91164849df-Abstract-Conference.html](http://papers.nips.cc/paper_files/paper/2022/hash/a94a8800a4b0af45600bab91164849df-Abstract-Conference.html).
- Tao, L., Feng, L., Yi, J., Huang, S., Chen, S., 2021. Better safe than sorry: Preventing delusive adversaries with adversarial training, in: Ranzato, M., Beygelzimer, A., Dauphin, Y.N., Liang, P., Vaughan, J.W. (Eds.), *Advances in Neural Information Processing Systems 34: Annual Conference on Neural Information Processing Systems 2021, NeurIPS 2021, December 6-14, 2021, virtual*, pp. 16209–16225. URL: <https://proceedings.neurips.cc/paper/2021/hash/8726bb30dc7ce15023daa8ff8402bcfd-Abstract.html>.
- van Vlijmen, D., Kolmus, A., Liu, Z., Zhao, Z., Larson, M.A., 2022. Generative poisoning using random discriminators. *CoRR abs/2211.01086*. URL: <https://doi.org/10.48550/arXiv.2211.01086>, doi:10.48550/ARXIV.2211.01086, arXiv:2211.01086.
- Wang, Z., Wang, Y., Wang, Y., 2021. Fooling adversarial training with inducing noise. *CoRR abs/2111.10130*. arXiv:2111.10130.
- Wen, R., Zhao, Z., Liu, Z., Backes, M., Wang, T., Zhang, Y., 2023. Is adversarial training really a silver bullet for mitigating data poisoning?, in: *The Eleventh International Conference on Learning Representations, ICLR 2023, Kigali, Rwanda, May 1-5, 2023*, OpenReview.net. URL: <https://openreview.net/pdf?id=zKvm1ETD0q>.
- Wu, S., Chen, S., Xie, C., Huang, X., 2022. One-pixel shortcut: on the learning preference of deep neural networks. *CoRR abs/2205.12141*. doi:10.48550/arXiv.2205.12141, arXiv:2205.12141.
- Wu, S., Chen, S., Xie, C., Huang, X., 2023. One-pixel shortcut: On the learning preference of deep neural networks, in: *The Eleventh International Conference on Learning Representations, ICLR 2023, Kigali, Rwanda, May 1-5, 2023*, OpenReview.net. URL: <https://openreview.net/pdf?id=p7G8t5FVn2h>.
- Yu, D., Zhang, H., Chen, W., Yin, J., Liu, T.Y., 2021. Indiscriminate poisoning attacks are shortcuts. arXiv preprint arXiv:2111.00898.
- Yuan, C., Wu, S., 2021. Neural tangent generalization attacks, in: Meila, M., Zhang, T. (Eds.), *Proceedings of the 38th International Conference on Machine Learning, (ICML), Virtual Event, PMLR*. pp. 12230–12240.
- Yun, S., Han, D., Chun, S., Oh, S.J., Yoo, Y., Choe, J., 2019. Cutmix: Regularization strategy to train strong classifiers with localizable features, in: *2019 IEEE/CVF International Conference on Computer Vision, ICCV 2019, Seoul, Korea (South), October 27 - November 2, 2019*, IEEE. pp. 6022–6031. URL: <https://doi.org/10.1109/ICCV.2019.00612>, doi:10.1109/ICCV.2019.00612.